Supplementary Information (SI) for Materials Horizons.
This journal is © The Royal Society of Chemistry 2024

Supporting Information

Cu-incorporated MIL-125-NH_2(Ti): A Versatile Visible-Light-Driven Platform for Enhanced Photocatalytic H_2 Generation and CO_2 Photoconversion

Anna Pancielejko [a], Mateusz A. Baluk [a], Hanna Zagórska [a], Magdalena Miodyńska-Melzer [a], Anna Gołąbiewska [a], Tomasz Klimczuk [b], Mirosław Krawczyk [c], Mirosława Pawlyta [d], Krzysztof Matus [d], Alicja Mikolajczyk [f,g], Henry P. Pinto [h], Aleksandra Pieczyńska [a], Joanna Dołżonek [e], Adriana Zaleska-Medynska [a*]*

[a] Department of Environmental Technology, Faculty of Chemistry, University of Gdansk, 80-309 Gdansk, Poland

[b] Faculty of Applied Physics and Mathematics and Advanced Materials Centre, Gdansk University of Technology, 80-233 Gdansk, Poland

[c] Institute of Physical Chemistry, Polish Academy of Sciences, 01-224 Warsaw, Poland

[d] Faculty of Mechanical Engineering, Silesian University of Technology, 44-100 Gliwice, Poland

[e] Department of Environmental Analysis, Faculty of Chemistry, University of Gdańsk, 80-309 Gdansk, Poland

[f] Laboratory of Environmental Chemoinformatics, Faculty of Chemistry, University of Gdansk, 80-308, Gdansk, Poland

[g] QSAR LAB, 80-172, Gdansk, Poland

[h] CompNano Group, School of Physical Sciences and Nanotechnology, Yachay Tech University, Urcuqui 100119, Ecuador

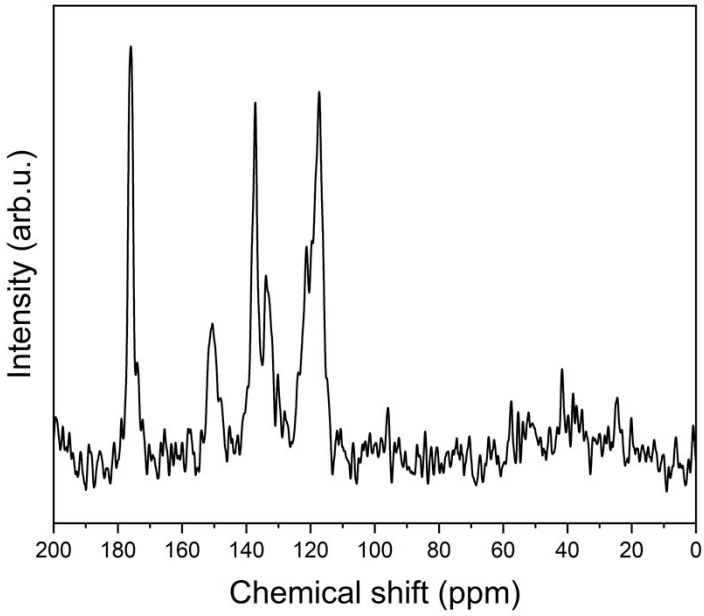

Figure S1. Solid state ^{13}C NMR of the MIL(Cu/Ti)1.0 photocatalyst.

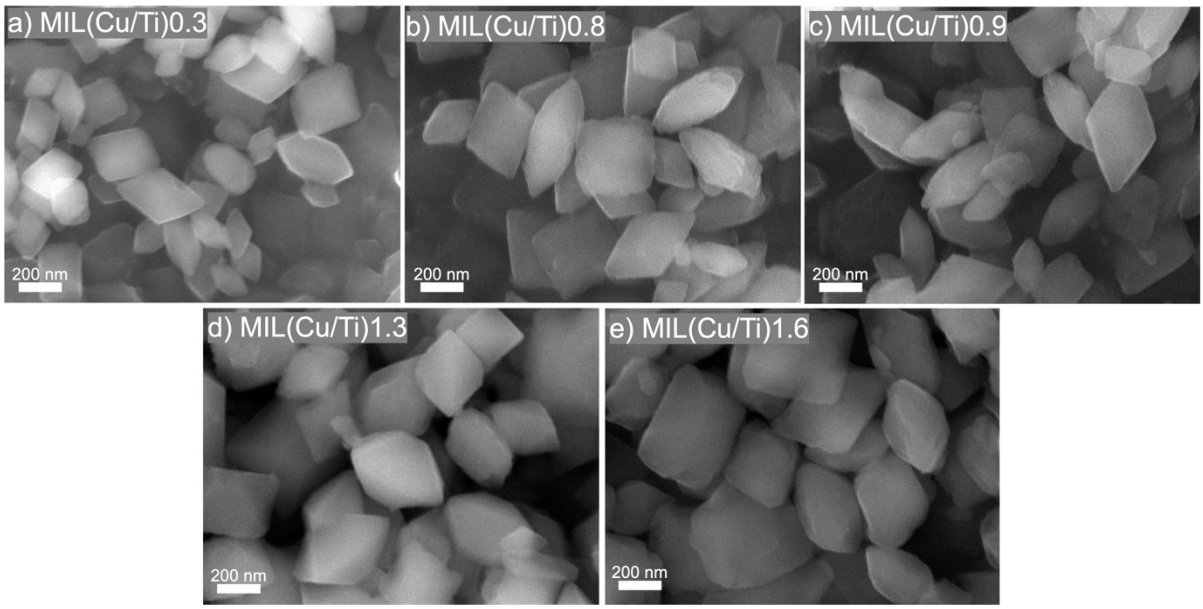

Figure S2. SEM images of the Cu-incorporated NH_2-MIL-125(Ti) samples.

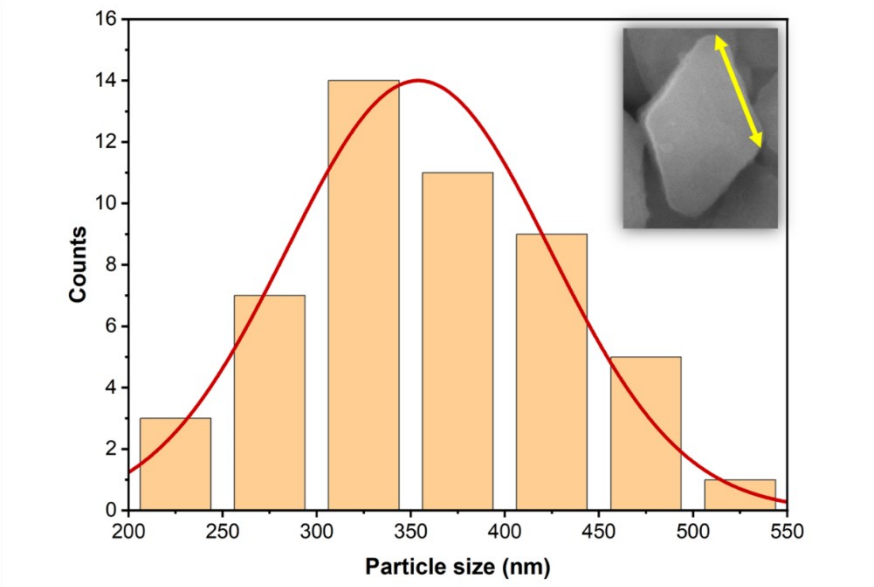

Figure S3. Particle size distribution was determined from 50 measured particles of pristine MIL(Ti). The image inside shows how the particle edge size was measured.

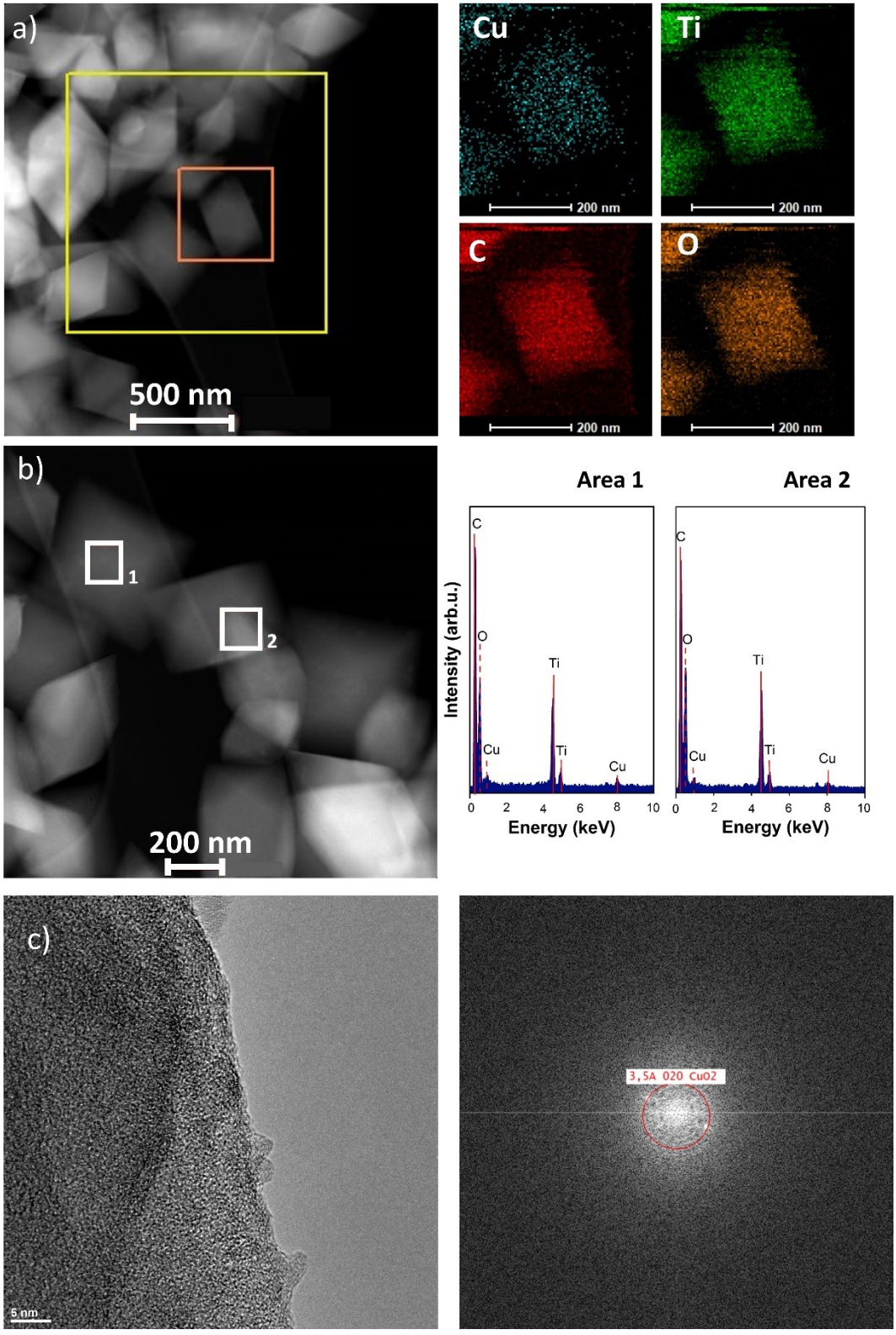

Figure S4. a) TEM image, and EDS elemental mapping for Cu, Ti, C, and O, b) EDX spectrum, and c) HRTEM image of the surface of MIL(Cu/Ti)1.6 sample.

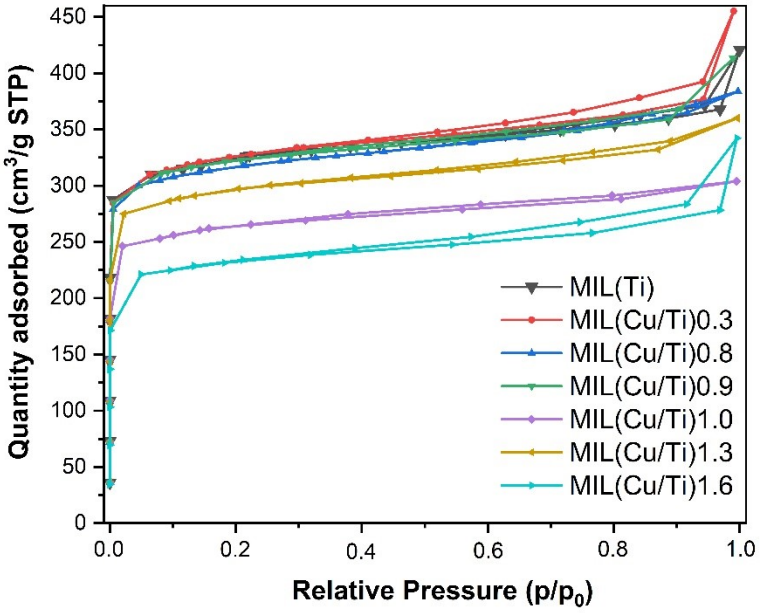

Figure S5. N_2 adsorption–desorption isotherms for pristine and Cu-modified MIL(Ti).

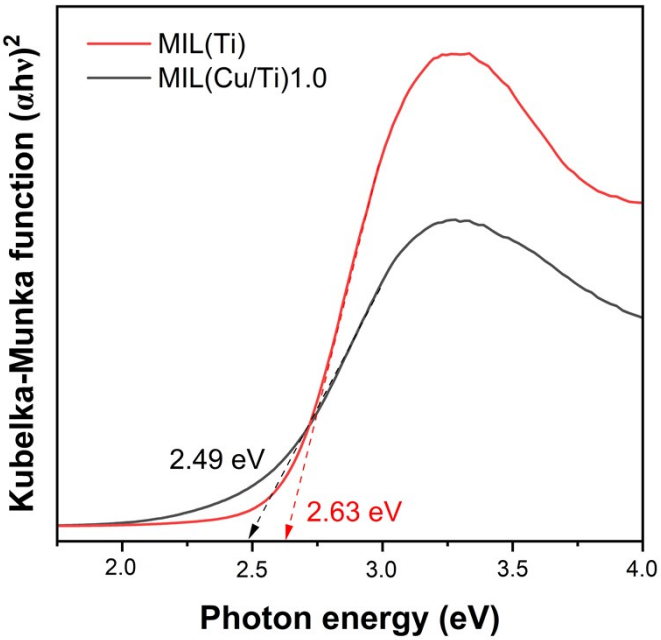

Figure S6. The band gap of pristine MIL(Ti) and MIL(Cu/Ti)1.0 through the Kubelka-Munk transformation method.

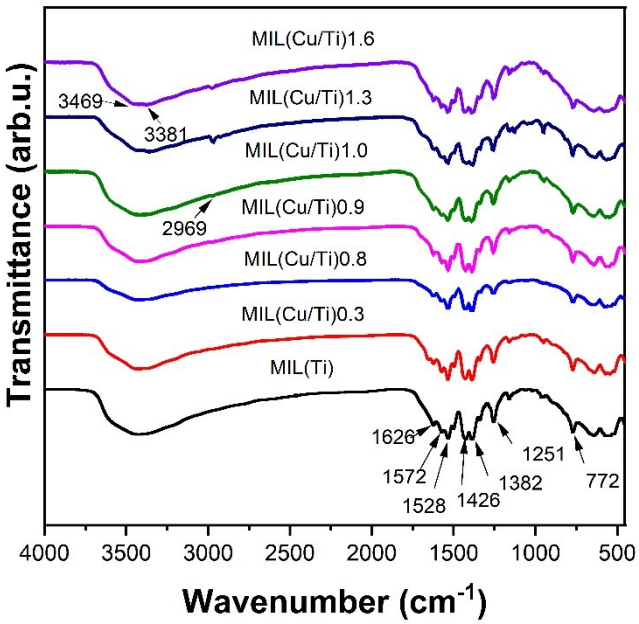

Figure S7. FT-IR spectra of pristine and Cu-incorporated NH_2-MIL-125(Ti) powders.

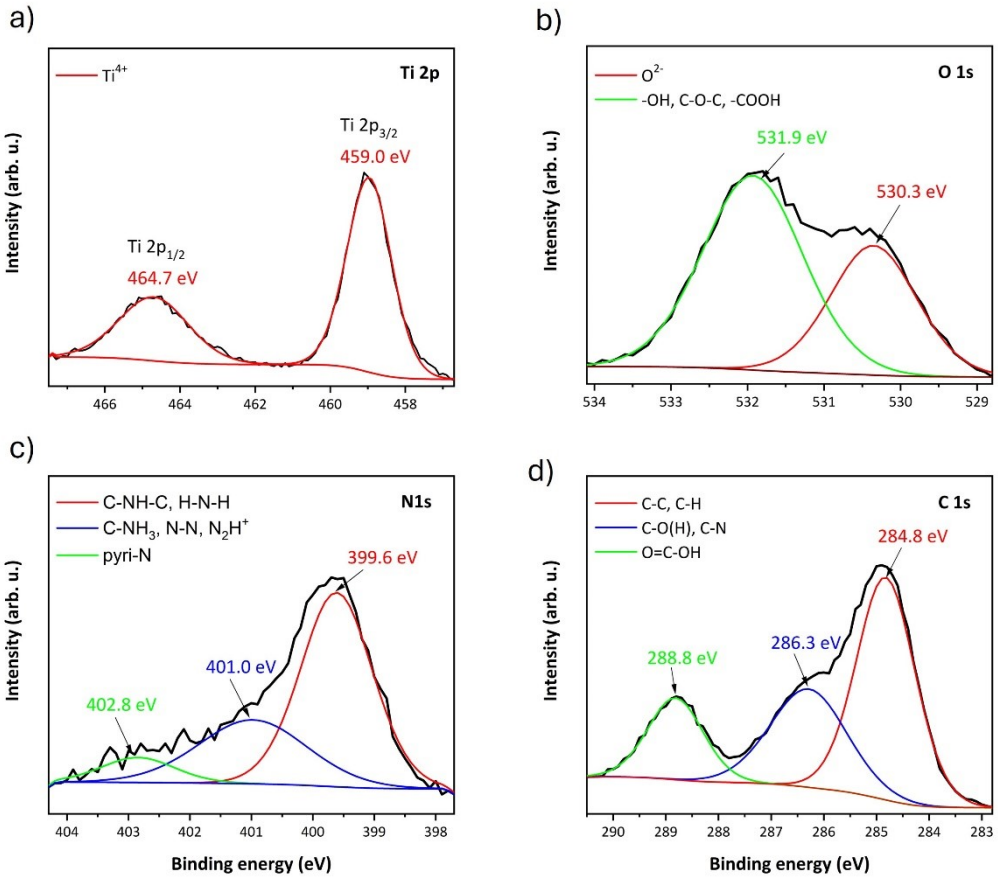

Figure S8. High-resolution (HR) XPS spectra of Ti 2p, O 1s, N 1s, and C 1s with chemical characteristics of the MIL(Ti) sample.

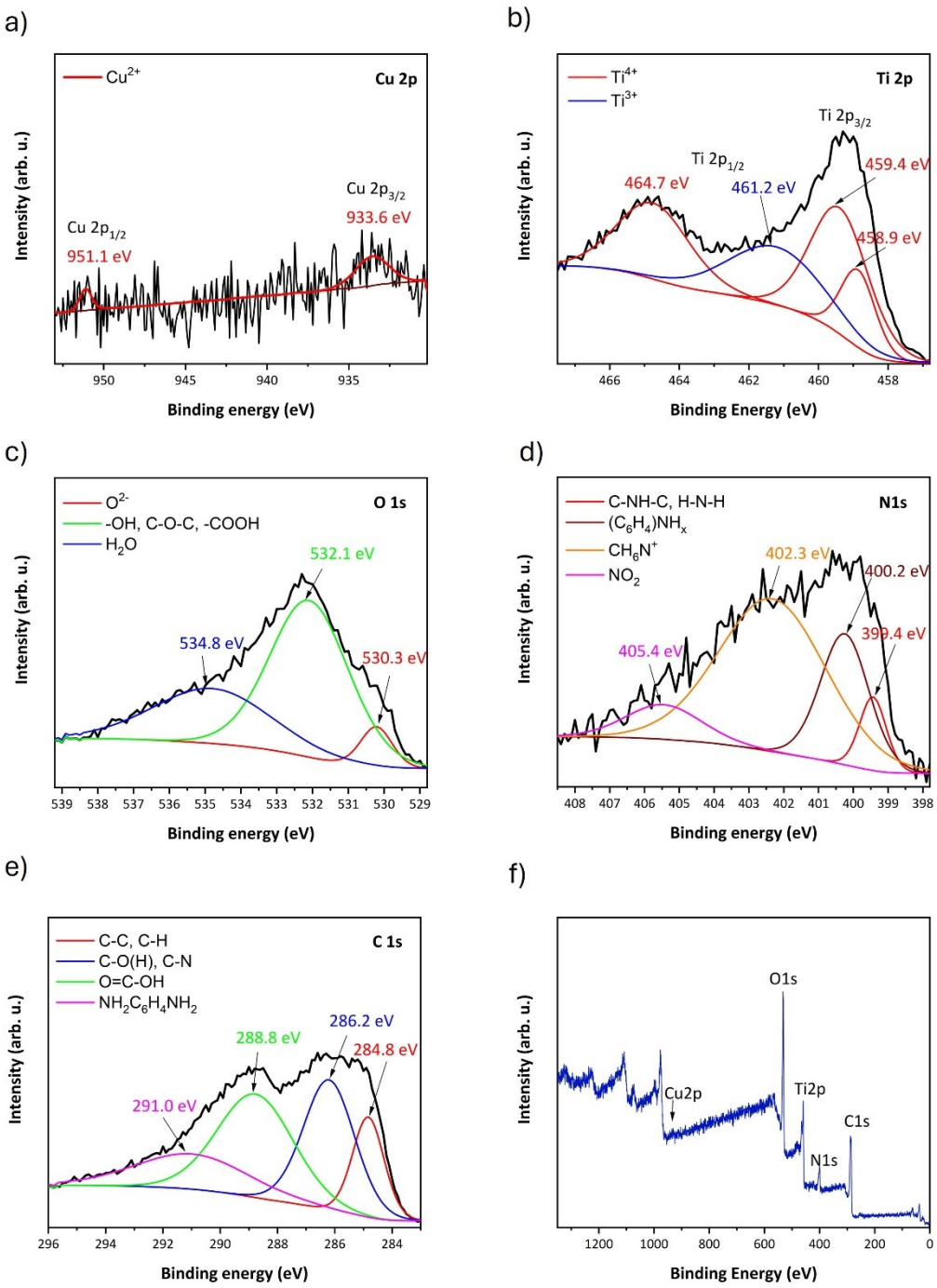

Figure S9. High-resolution (HR) XPS spectra of Cu 2p, Ti 2p, O 1s, N 1s, and C 1s with chemical characteristics and survey spectrum of the MIL(Cu/Ti)0.3 sample.

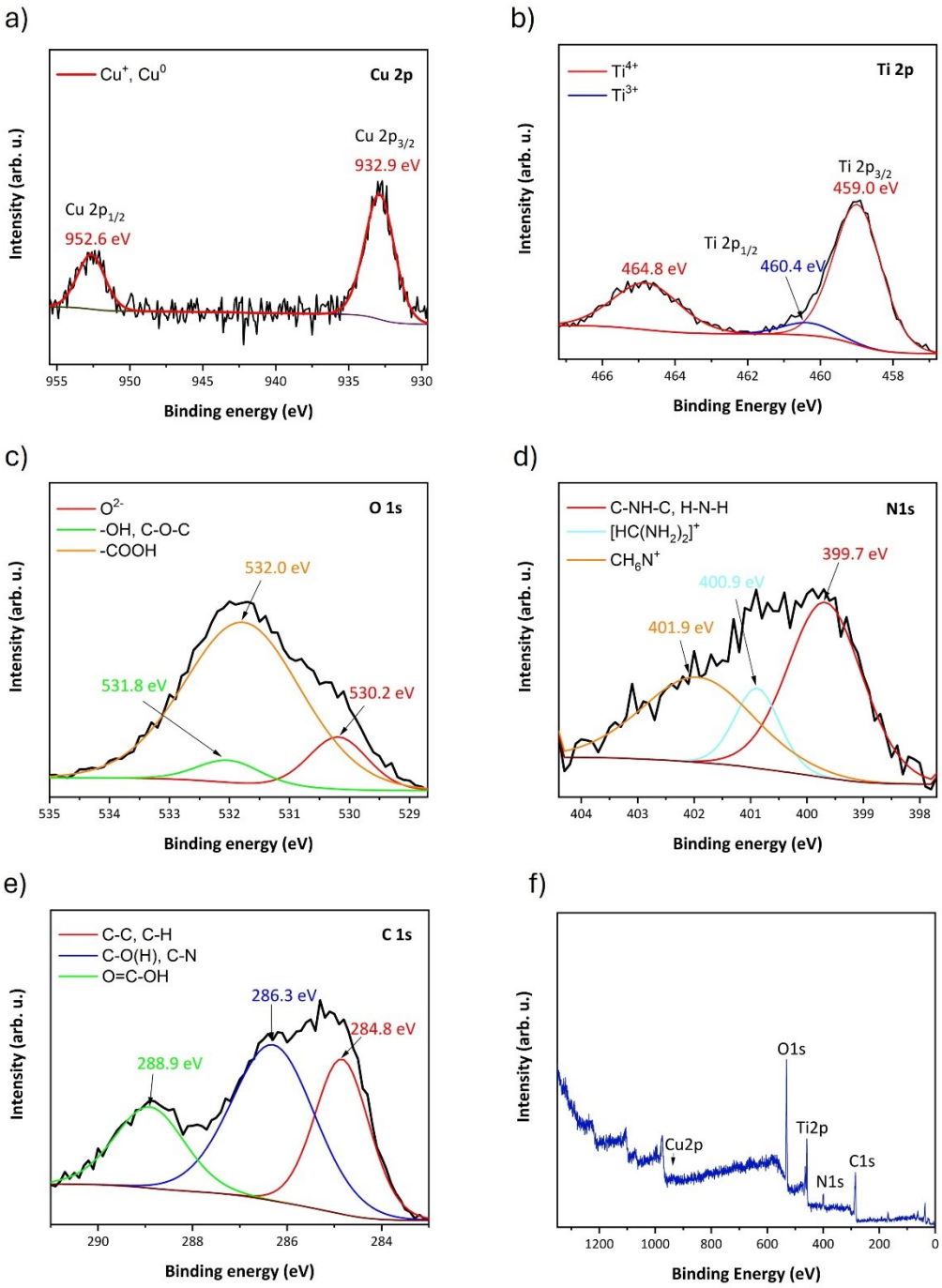

Figure S10. High-resolution (HR) XPS spectra of Cu 2p, Ti 2p, O 1s, N 1s, and C 1s with chemical characteristics and survey spectrum of the MIL(Cu/Ti)1.6 sample.

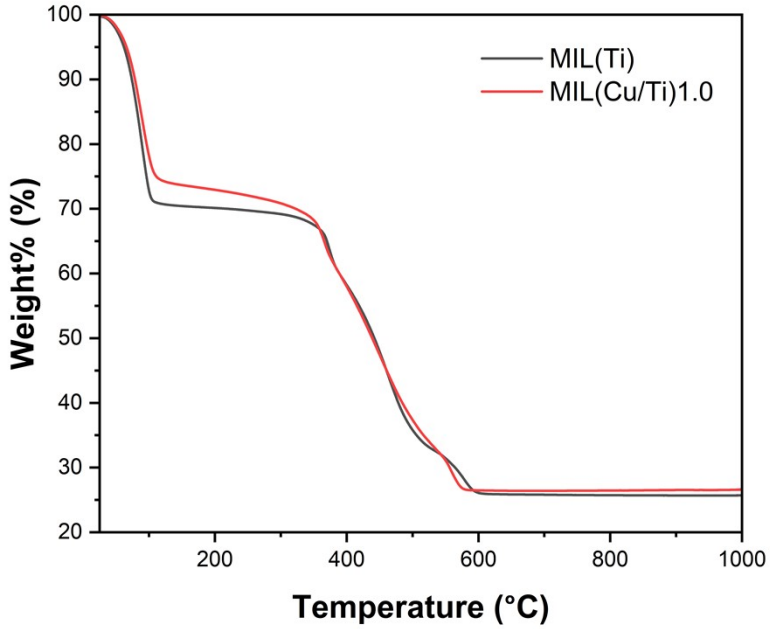

Figure S11. The TG analysis of pristine MIL(Ti) and MIL(Cu/Ti)1.0 photocatalysts in the range of 28°C to 1000°C at a heating rate of 10°C/min.

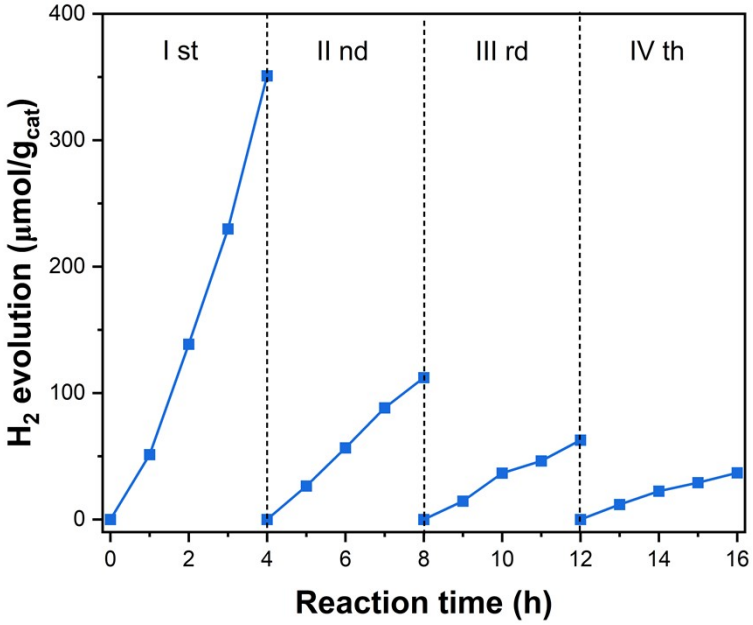

Figure S12. Cyclic stability test of H_2 generation over MIL(Cu/Ti)1.0 photocatalyst under UV-Vis irradiation.

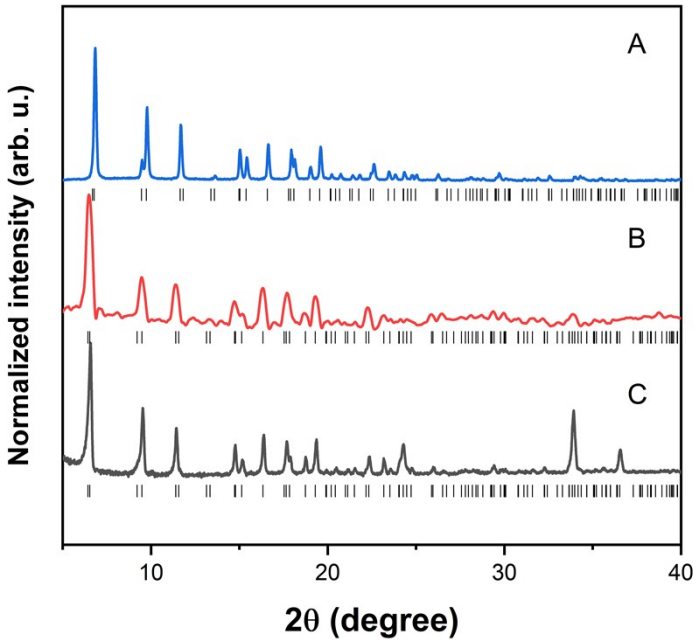

Figure S13. XRD patterns of pristine MIL(Ti): A – before the irradiation, B – after 4 hours of the UV-Vis irradiation, and C - after 4 hours of the Vis irradiation.

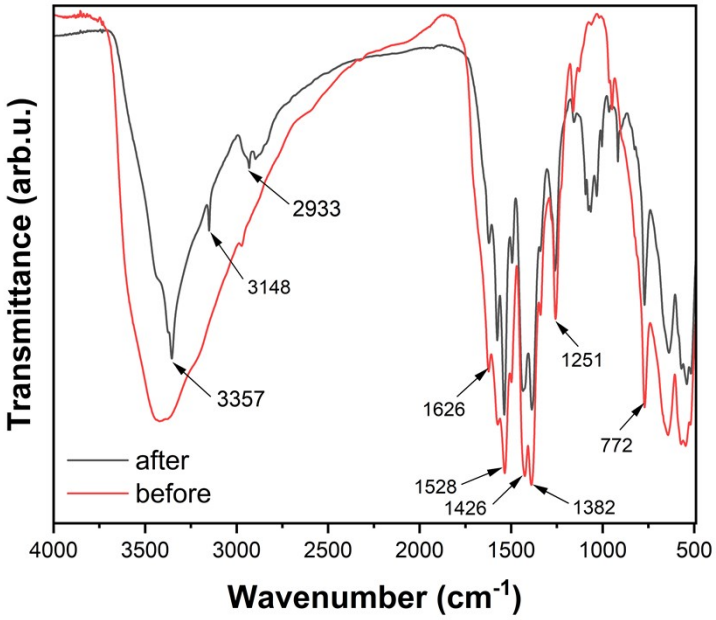

Figure S14. FT-IR spectra of the MIL(Cu/Ti)1.0 after the photoreaction of H_2 generation under UV-Vis irradiation.

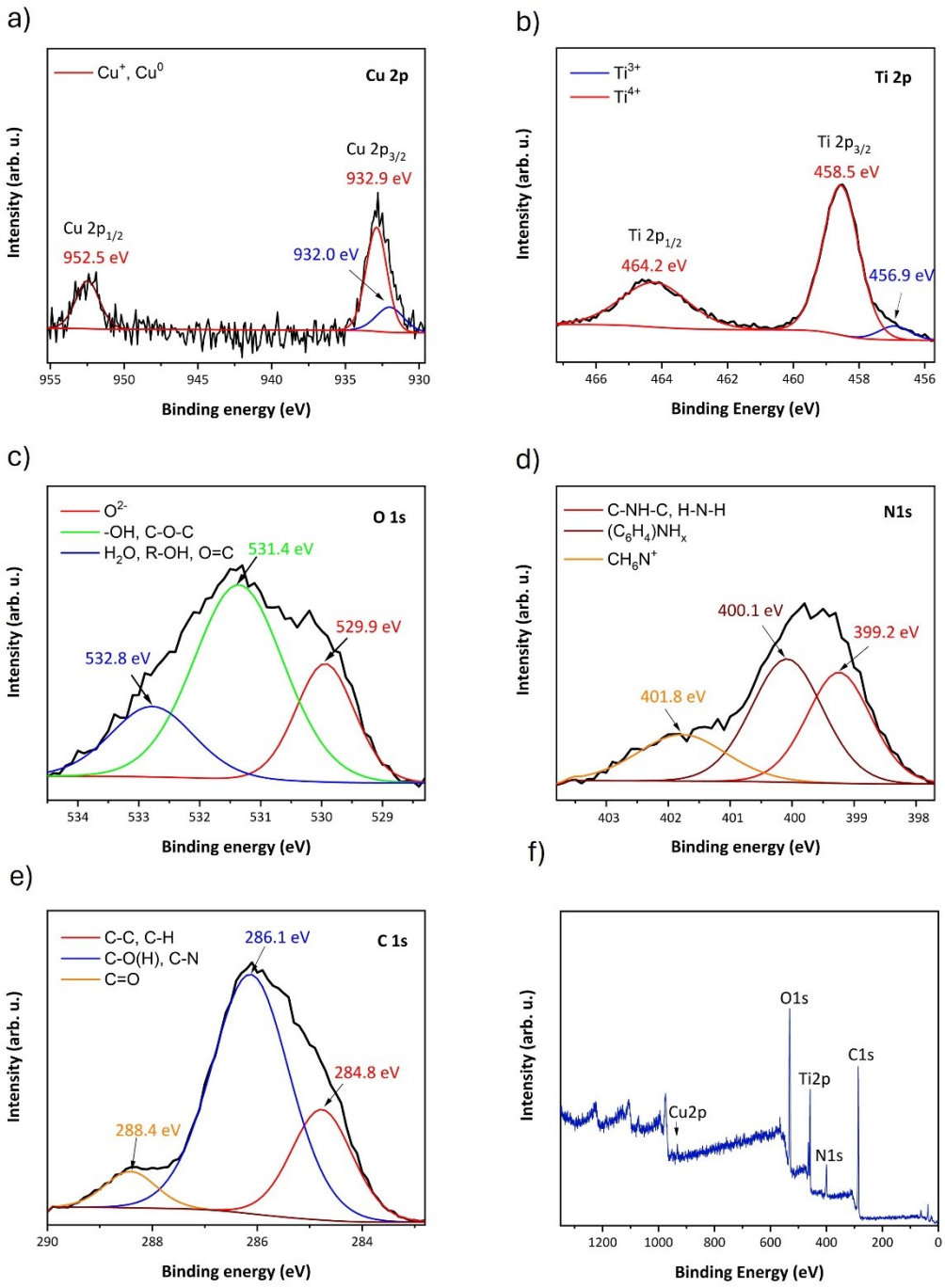

Figure S15. High-resolution (HR) XPS spectra of Cu 2p, Ti 2p, O 1s, N 1s, and C 1s with chemical characteristics and the MIL(Cu/Ti)1.0 survey spectrum after 4 hours of UV-Vis irradiation.

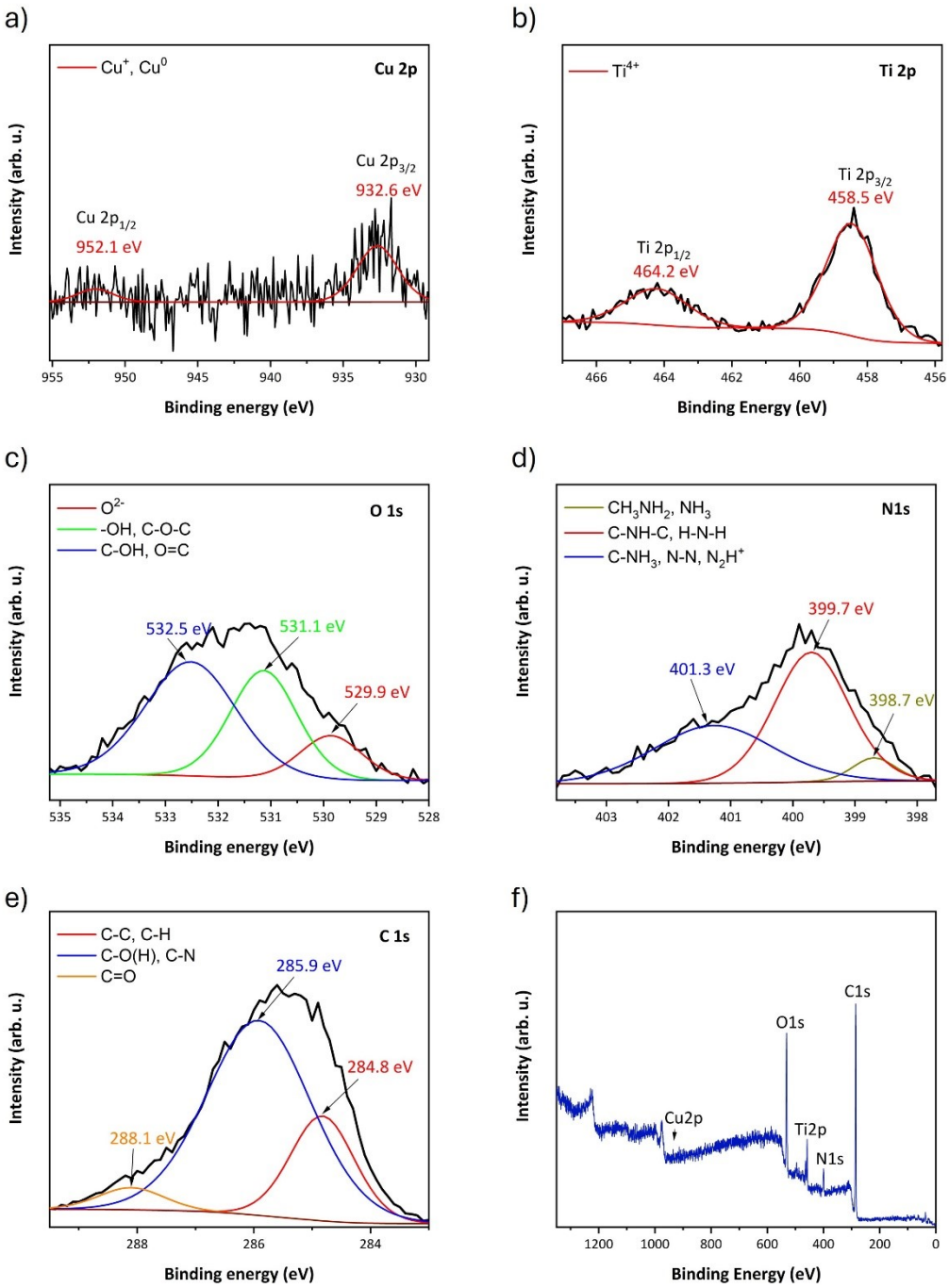

Figure S16. High-resolution (HR) XPS spectra of Cu 2p, Ti 2p, O 1s, N 1s, and C 1s with chemical characteristics and the MIL(Cu/Ti)1.0 survey spectrum after 4 hours of visible light irradiation.

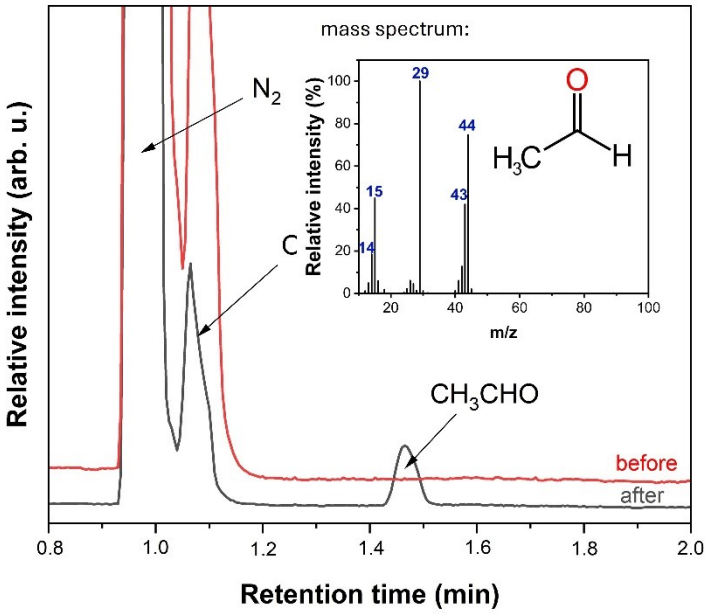

Figure S17. Headspace GC/MS spectra of the electrolyte before (red line) and after (black line) 4 h of the visible light irradiation during H_2 generation photoprocess using MIL(Cu/Ti)1.0 sample (AcN/TEOA/H_2O 18/2/0.3, v/v/v) with signals detected for acetaldehyde.

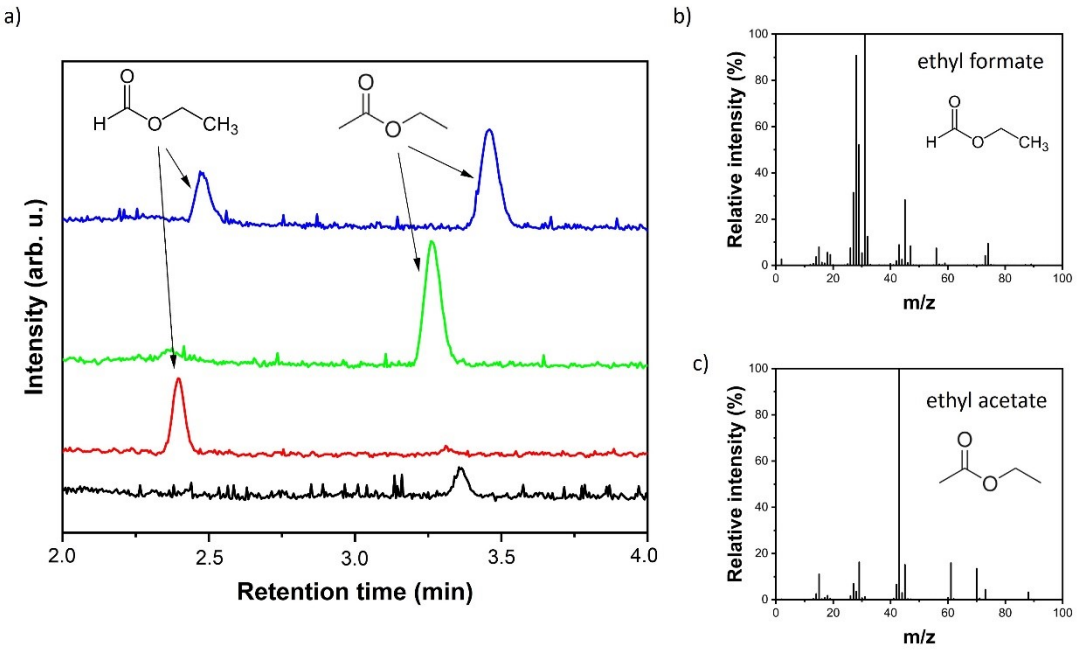

Figure S18. a) Headspace GC/MS spectra of the obtained samples: black line - electrolyte (AcN/TEOA, 9/1, v/v), red line – reference solution of HCOOH (500 μM), green line - photoconversion product of $^{12}CO_2$ after 4 h in the N_2 atmosphere using MIL(Cu/Ti)1.0, and blue line - photoconversion product of $^{13}CO_2$ after 4 h in the $^{13}CO_2$ atmosphere using MIL(Cu/Ti)1.0. Mass spectra of b) ethyl formate, and c) ethyl acetate after photoconversion of CO_2 using MIL(Cu/Ti)1.0.

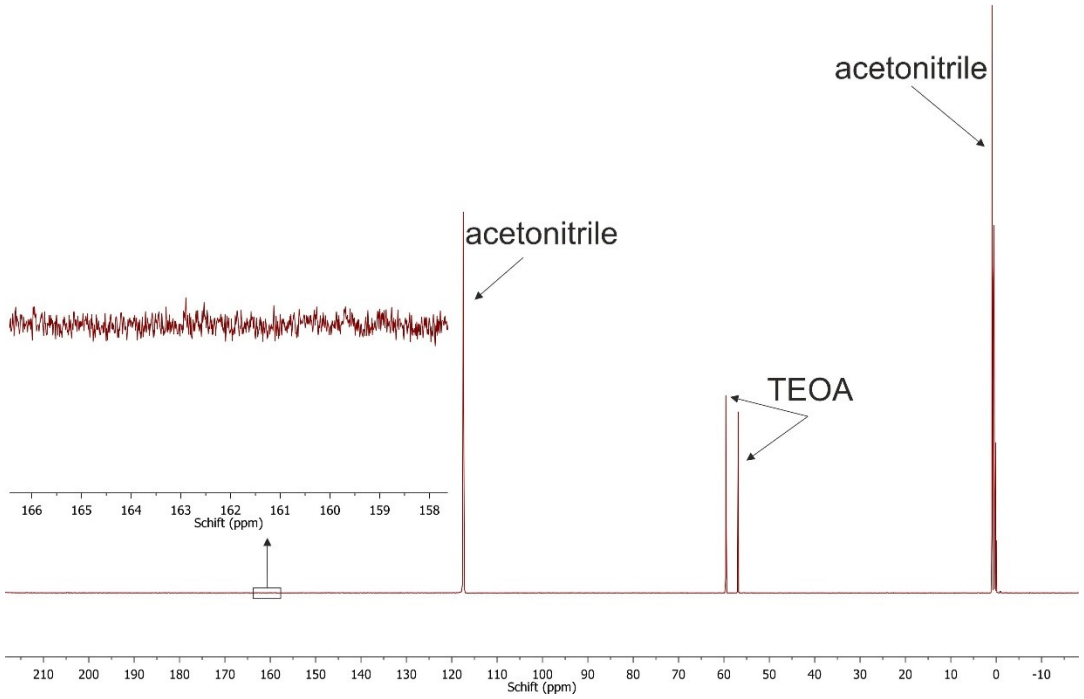

Figure S19. The ^{13}C NMR spectra of the products detected for the ^{12}C standard solution.

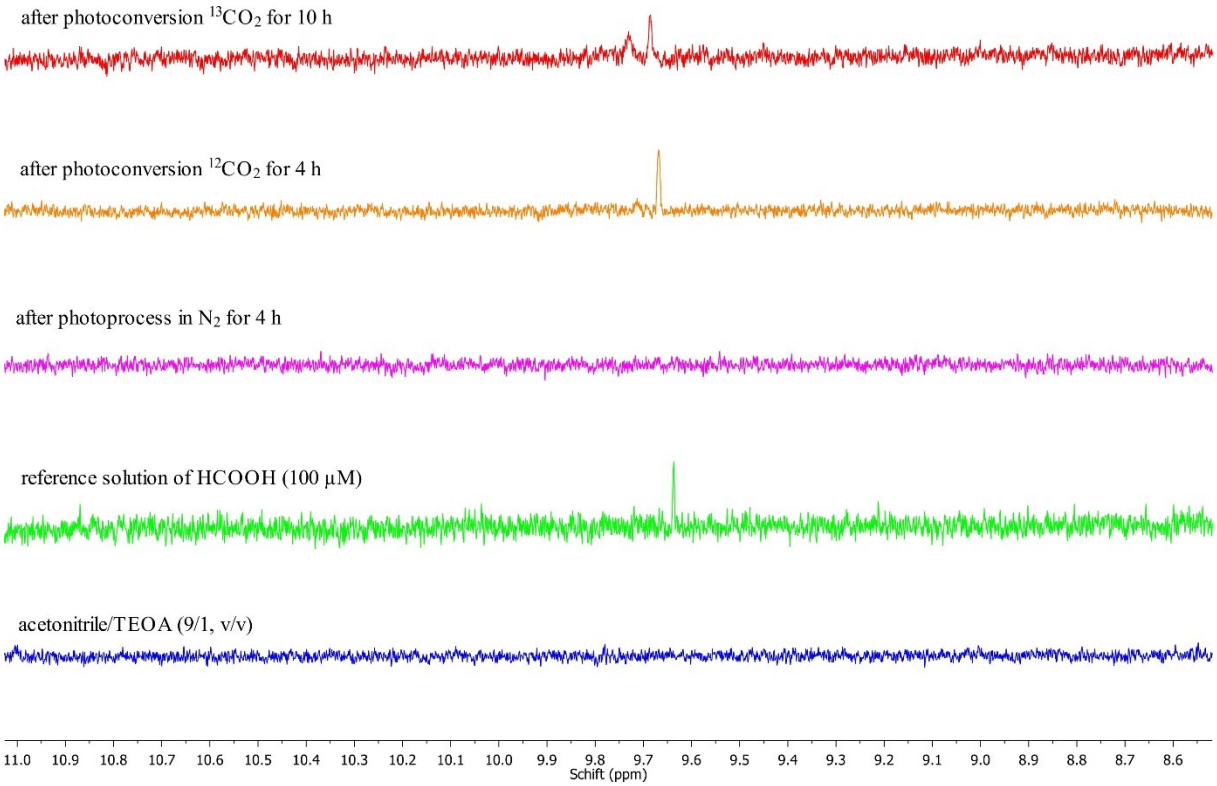

Figure S20. ^{1}H NMR spectra of pristine electrolyte (AcN/TEOA), HCOOH standard solution, and products of CO_2 photoconversion for 2 h in CO_2 and N_2 over MIL(Cu/Ti) under visible-light irradiation.

Table S1. Comparison of the most important data on photocatalytic H_2 generation in the presence of NH_2-MIL-125(Ti)-based compounds with the results from this study.

Sample label	Photocatalytic H_2 generation				Yield/rate	Ref.
	Photocatalyst mass (mg)	Electrolyte composition	Irradiation time (h)	Light source		
Ru-MIL-125-NH_2	10	AcN/H_2O/TEAO (18/2/0.3, v/v/v)	n/a	300 W Xe lamp (>420 nm)	426 μmol h^{-1} g^{-1}	[1]
Pt/NH_2-MIL-125(Ti)	50	AcN/TEOA (5/1, v/v)	8	300 W Xe lamp (>420 nm)	235 μmol	[2]
2%CuNPs/d-NH_2-MIL-125	3	AcN/H_2O/TEAO (4/1/0.2, v/v/v)	4	300 W Xe lamp (>420 nm)	1326.55 mmol g^{-1} h^{-1}	[3]
Co(II)@MIL-125-NH_2	6	ACN/TEOA/H_2O (27.6/1.4/1, v/v/v)	2.5	300 W Xe lamp (>380 nm)	553 μmol g^{-1} h^{-1}	[4]
Co@NH_2-MIL-125	5	AcN/TEA/H_2O (5/1/0.1, v/v/v)	n/a	500 W Hg/Xe lamp(>408 nm)	0.62 mmol h^{-1} g^{-1}	[5]
Pd-MIL-125-NH_2	50	H_2O/HCOOH/HCOONa (4.6 mL/0.39 mL/0.54 g)	3	n/a	0.320 mmol h^{-1} g^{-1}	[6]
Co@NH_2-MIL-125(Ti)	30	AcN/TEA/H_2O (23.5/4.7/0.5, v/v/v)	22.5	500 W Xe/Hg lamp (λ>385 nm)	900 μmol/g_{cat}	[7]
MIL(Cu/Ti)1.0	25	ACN/TEOA/H_2O (18/2/0.3, v/v/v)	4	1000 W Xe lamp (>420 nm)	127 μmol/g_{cat}	This work

n/a not available

Table S2. Comparison of the most important data on photocatalytic CO_2 generation in the presence of NH_2-MIL-125(Ti)-based compounds with the results from this study.

Sample label	Photocatalytic CO_2 photoconversion				Yield/rate	Ref.
	Photocatalyst mass (mg)	Electrolyte composition	Irradiation time (h)	Light source		
NH_2-MIL-125(Ti)	50	AcN/TEOA (5/1, v/v)	10	500 W Xe lamp (>420 nm)	HCOOH: 8.14 µmol	[8]
Co/NH_2-MIL-125(Ti)	50	AcN/TEOA (5/1, v/v)	10	300 W Xe lamp (>420 nm)	HCOOH: 38.4 µmol h^{-1} g_{cat}^{-1}	[9]
Pt/NH_2-MIL-125(Ti)	50	AcN/TEOA (5/1, v/v)	8	300 W Xe lamp (>420 nm)	HCOOH: 12.96 µmol	[2]
rGO@NH2-MIL-125	30	MeOH	4	250W high-pressure mercury lamp	HCOOH: 1.116 µmol g^{-1} h^{-1}	[10]
MOF_met_0.5%Cu	50	AcN/TEOA (9/1, v/v),	4	1000 W Xe lamp (>420 nm)	HCOOH: 30.1 µmol g^{-1} h^{-1}	[11]
MIL(Cu/Ti)1.0	25	ACN/TEOA (9/1, v/v)	4	1000 W Xe lamp (>420 nm)	HCOOH: 62.4 µmol/g_{cat}	This work

Table S3. Surface elemental composition (in at.%) of MIL(Cu/Ti)1.0 sample after the photocatalytic H_2 generation after 4 hours of UV-Vis and Vis irradiation evaluated by XPS.

Sample label	at.% (in total)					
	C	Ti	O	N	Cu	Na
MIL(Cu/Ti)1.0 after UV-Vis irradiation	61.9	5.5	24.1	7.6	0.1	0.8
MIL(Cu/Ti)1.0 after Vis irradiation	73.9	2.3	17.3	6.0	0.1	0.8

Table S4. Efficiency of CO_2 photoconversion to HCOOH using the obtained samples under visible-light irradiation.

Sample label	CO_2 photoconversion	
	Yield of HCOOH product ($\mu mol/g_{cat}$)	Yield of HCOOH product ($\mu mol/g_{cat} \cdot h$)
MIL(Ti)	dl	dl
MIL(Cu/Ti)0.3	dl	dl
MIL(Cu/Ti)0.8	11.6	2.9
MIL(Cu/Ti)0.9	25.3	6.3
MIL(Cu/Ti)1.0	62.4	15.6
MIL(Cu/Ti)1.3	42.7	10.7
MIL(Cu/Ti)1.6	32.6	8.1

* dl – below the limit of detection

Table S5. CO_2 sorption at ~1 bar (p/p_0 ~0.97).

Sample label	CO_2 capacity (mmol/g)	Heat of CO_2 adsorption (kJ/mol)
MIL(Ti)	2.56	16.3
MIL(Cu/Ti)0.3	2.40	21.1
MIL(Cu/Ti)0.8	2.20	21.6
MIL(Cu/Ti)0.9	2.41	20.4

MIL(Cu/Ti)1.0	2.06	22.6
MIL(Cu/Ti)1.3	2.45	20.2
MIL(Cu/Ti)1.6	1.84	22.1

Testing the PBE/HSE06 and PBEsol/HSEsol for MIL-125(Ti) and NH_2-MIL-125(Ti)

We tested the final electronic structure using the fully relaxed crystal structures of pristine MIL-125(Ti) and NH_2-MIL-125(Ti) using a combination of the functionals PBE with HSE06 as well as PBEsol with HSEsol[12–14], as implemented in VASP[15,16]. In all the cases, the convergency of < 1meV/atom is achieved utilizing a cutoff energy of 850 eV and the Γ-point.

First, we computed the crystal and electronic structure of pristine MIL-125(Ti). In short, this porous crystal structure is composed by twelve BDC linkers and sixteen TiO_6 octahedral units as displayed in Figure S21. Table S4 shows the computed cell parameters and predicted band gap E_g. Figure S22, displays a direct comparison between the PBE/HSE06 and PBEsol/HSEsol partial density of states (PDOS), here we aligned the energy to the computed vacuum level for each system. The results are in agreement with the experiments. The VB comprises abc-linker states with C-2p and O-2p states, and the CB is composed of the Ti-3d and O-2p of the TiO_2 octahedral states.

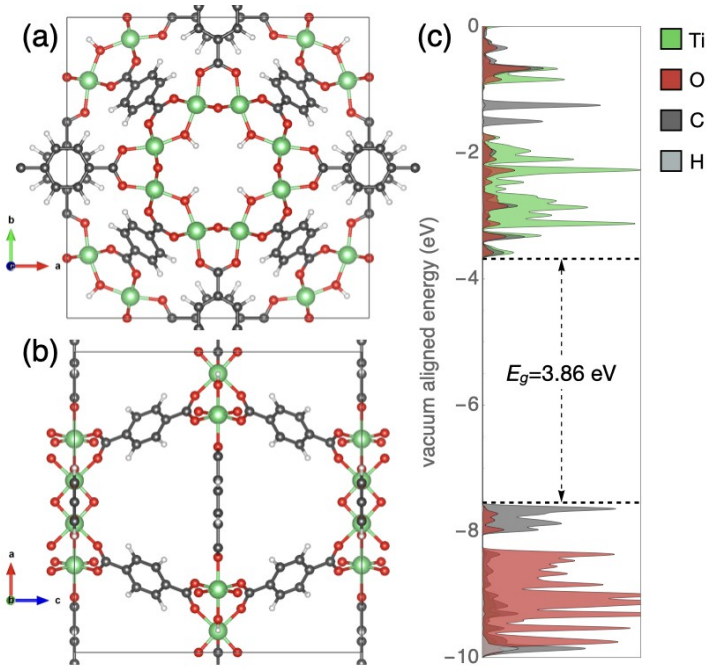

Figure S21. (a,b) PBEsol computed crystal structure of pristine MIL-125(Ti)), the black box denotes the unit cell, and (c) PBEsol/HSEsol computed PDOS. The atoms and corresponding PDOS are colored as follows: Ti(green), O(red), C(gray), and H(light gray).

Table S6. PBE and PBEsol predicted cell parameters and electronic properties for MIL-125(Ti). Experiment data are from Ref[17]. The E_g values are computed using PBE/HSE06 and PBEsol/HSEsol.

Method	a=b (Å)	c (Å)	α=β=γ (°)	V (Å^3)	E_g (eV)
PBE/HSE06	19.02426	18.07255	90	6540.859	3.86
PBEsol/HSEsol	18.88122	17.94032	90	6395.736	3.82
Expt.	18.654	18.144	90	6313.599	3.6

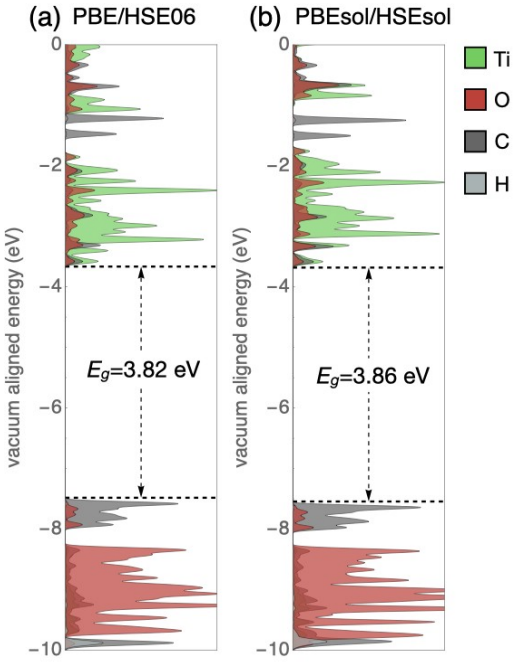

Figure S22. Computed (a) PBE/HSE06 and (b) PBEsol/HSEsol PDOS for MIL-125(Ti). The results suggest that both functional combinations produce the same electronic structure for MIL-125(Ti). The PDOS are colored as follows: Ti(green), O(red), C(gray), and H(light gray).

Next, we computed the crystal and electronic structure of pristine NH_2-MIL-125(Ti). The initial structure was retrieved from Refs.[17,18]. In short, this crystal structure has twelve aminated NH_2-BDC linkers and twelve TiO_6 octahedral sites as displayed in Figure S23. Table S5 displays the cell parameters and predicted band gap E_g. Figure S24, displays a direct comparison between the PBE/HSE06 and PBEsol/HSEsol partial density of states (PDOS), here we aligned the energy to the computed vacuum level for each system. The presence of the amino group produces a subband at ~ -6 eV, where now it is located in the VB and is composed of N-2p and C-2p states.

The CB is not affected by the aminated linker and is composed of the Ti-3d and O-2p states, similar to the MIL-125(Ti) case. The overall effect of the NH_2-BDC in the electronic structure effectively reduces the band gap to 2.37 eV (Figure S24).

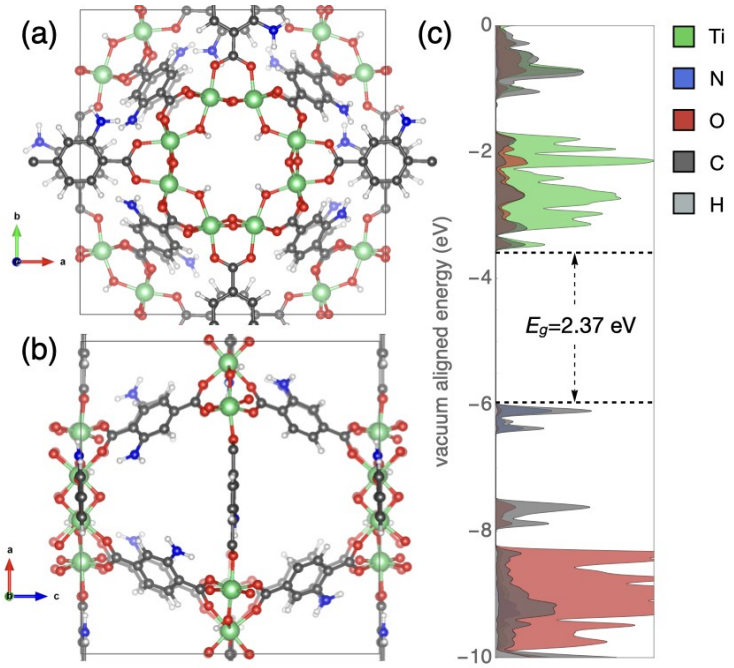

Figure S23. (a,b) PBEsol computed crystal structure of pristine NH_2-MIL-125(Ti), the black box denotes the unit cell, and (c) PBEsol/HSEsol computed PDOS. The atoms and corresponding PDOS are colored as follows: Ti(green), N(blue), O(red), C(gray), and H(light gray).

Table S7. PBE and PBEsol predicted cell parameters and electronic properties for pristine NH_2-MIL-125(Ti). The experimental cell parameters are from Ref.[17]. The E_g values are computed using PBE/HSE06 and PBEsol/HSEsol. The experimental E_g corresponds to Figure S6.

Method	*a* (Å)	*b* (Å)	*c* (Å)	α (°)	β (°)	γ (°)	*V* (Å^3)	E_g (eV)
PBE/HSE06	19.02371	19.00056	18.08259	89.62	89.85	90.01	6535.992	2.34
PBEsol/HSEsol	18.85378	18.87503	17.93825	89.92	89.99	89.96	6383.598	2.37
Expt.	18.729(3)	18.729(3)	18.172(4)	-	-	-	-	2.63
Calculated	18.680(1)	18.680(1)	18.149(1)	-	-	-	-	2.63

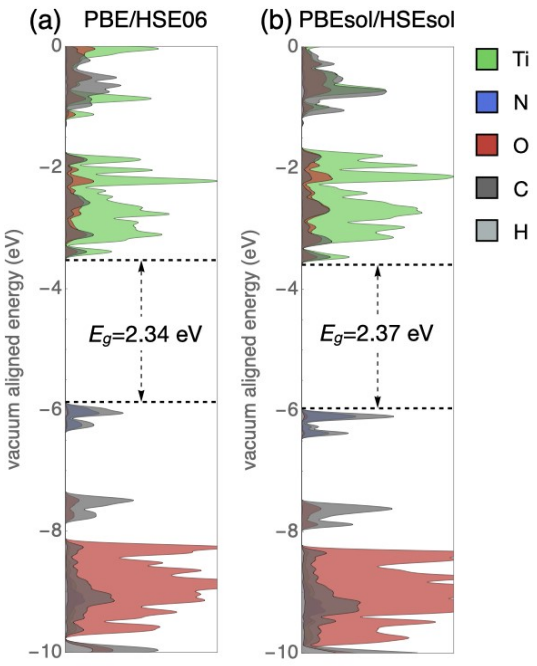

Figure S24. Computed (a) PBE/HSE06 and (b) PBEsol/HSEsol PDOS for pristine NH_2-MIL-125(Ti). The results suggest that both functional combinations produce practically the same electronic structure. The PDOS are colored as follows: Ti(green), N(blue), O(red), C(gray), and H(light gray).

These results suggest that PBE/HSE06 and PBEsol/HSEsol produce similar results. Therefore, in the following theoretical models, we decided to use PBEsol/HSEsol. It is important to stress that PBEsol functional was designed to produce better prediction when applied in bulk materials[12].

Electronic structure of MIL(Cu/Ti)1.0

Figures S25 and S26 display the fully relaxed supercells we considered to model the experimental case MIL(Cu/Ti)1.0. From an energetic point of view, our method is unable to solve which configuration is more stable since the energy difference between M1 and M2 is below our convergency criteria of 1 meV/atom. In both cases, the Cu doping on Ti sites produces a shallow electronic level at ~4 eV, becoming the new CB with Cu-3d and O-2p character. The VB at -6 eV is unaffected where the subband comprises Ti-3d and O-2p states similar to the pristine NH_2-MIL-125(Ti). The predicted band gap is ~1.8 eV.

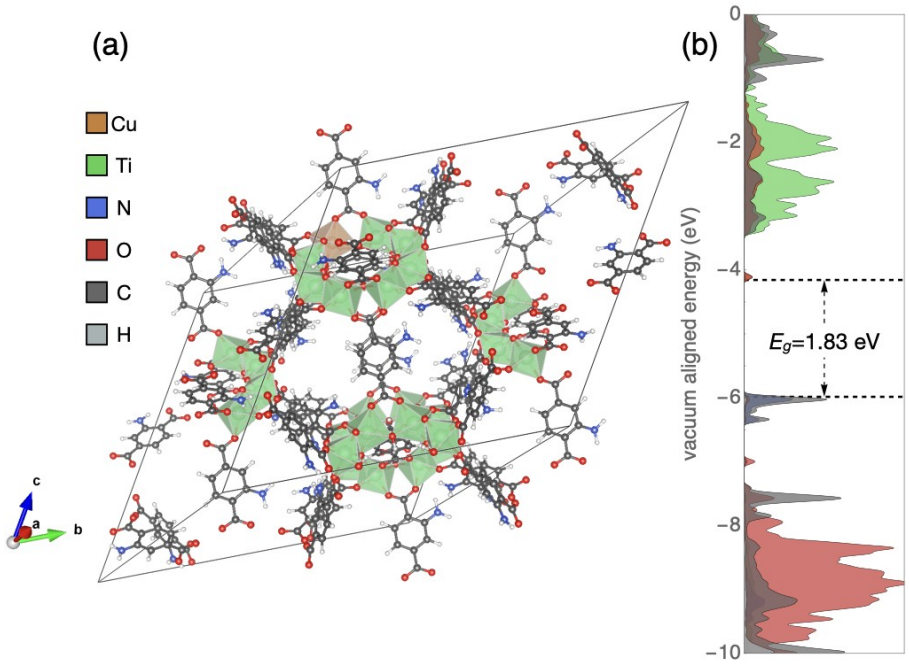

Figure S25. (a) PBEsol computed the crystal structure of MIL(Cu/Ti)1.0 M1 system, the black box denotes the supercell, and (b) PBEsol/HSEsol computed PDOS. The atoms and corresponding PDOS are colored as follows: Cu(orange), Ti(green), N(blue), O(red), C(gray), and H(light gray).

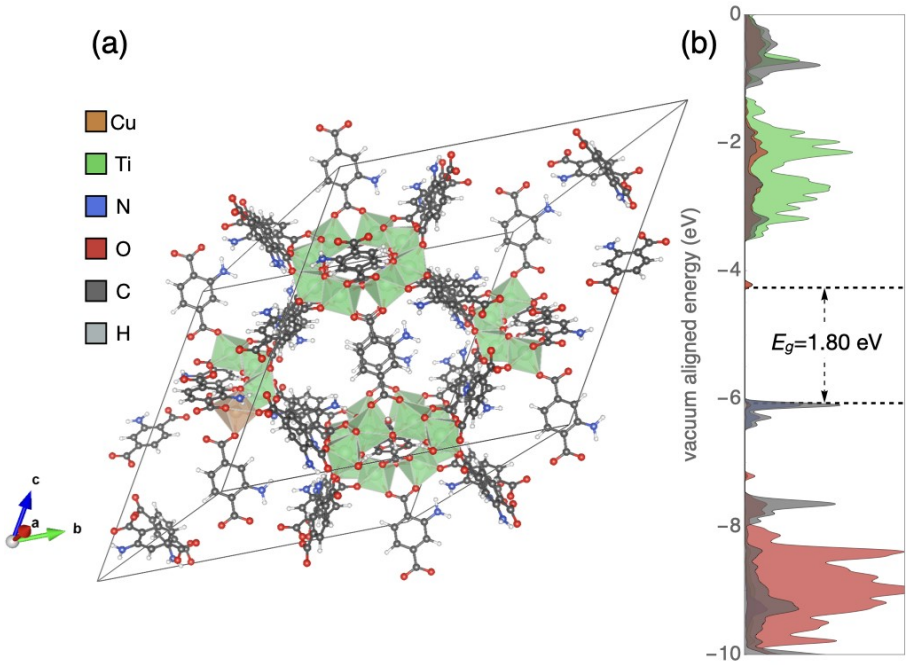

Figure S26. (a) PBEsol computed the crystal structure of MIL(Cu/Ti)1.0 M2 system, the black box denotes the supercell, and (b) PBEsol/HSEsol computed PDOS. The atoms and corresponding PDOS are colored as follows: Cu(orange), Ti(green), N(blue), O(red), C(gray), and H(light gray).

Finally, in Figure S27, we display the direct comparison of the PBEsol/HSEsol computed PDOS between the MIL-125(Ti), NH_2-MIL-125(Ti), and the MIL(Cu/Ti)1.0 models M1 and M2. The overall trend agrees with the experiments, and the Cu doping effectively affects only the CB, lowering the bandgap of the pristine NH_2-MIL-125(Ti).

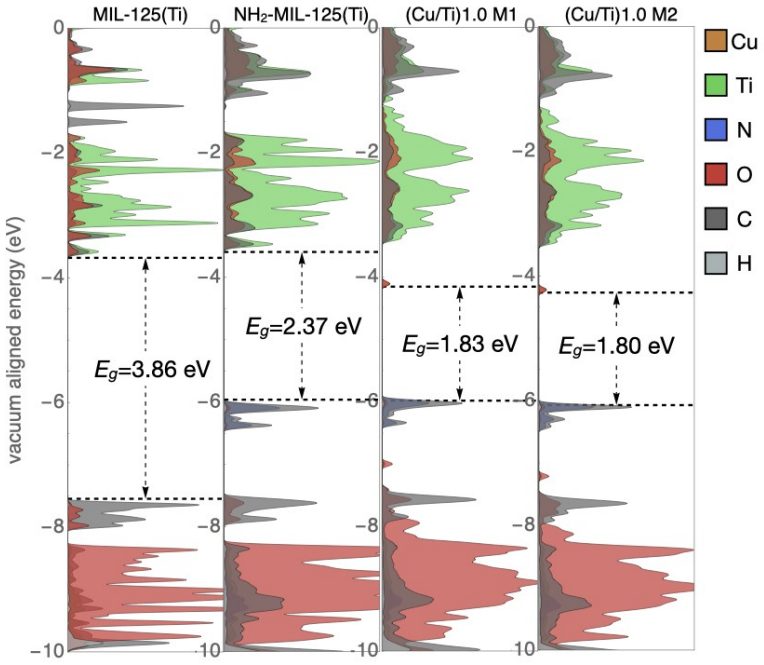

Figure S27. Computed PBEsol/HSEsol PDOS for pristine MIL-125(Ti), NH_2-MIL-125(Ti), and MIL(Cu/Ti)1.0 modeled by M1 and M2 supercells. The PDOS are colored as follows: Cu(orange), Ti(green), N(blue), O(red), C(gray), and H(light gray).

Following the method from Ref.[19], Table S6 details the PBEsol/HSEsol and PBE/HSE06 computed values of the spherical average of the electrostatic potential at the center of the pore sampled with a radius of 2 Å, here denoted as $V_{cen.}$, the ionization potential IP that considers the Janak's theorem[20] and using the computed Kohn-Sham eigenvalues[21]. The ionization potential is obtained by the relation EA=IP-E_g; we also include the statistical variance Var of the electrostatic potential within the 2 Å radius sphere; this value should be small, this means that the electrostatic potential around the pore is a plateau and a good representation of the vacuum level[19].

Table S8. PBEsol/HSEsol computed electrostatic potential at the pore center $V_{cen.}$, ionization potential IP, electron affinity EA, the band gap $E_{g,}$ and the statistical variance of the electrostatic potential Var. The values within parenthesis are the corresponding PBE/HSE06 computed values.

System	$V_{cen.}$(eV)	IP (eV)	EA (eV)	E_g (eV)	Var (V)
MIL-125(Ti)	3.05 (2.99)	7.54 (7.48)	3.68 (3.66)	3.86 (3.82)	1.8×10^{-5} (9.0×10^{-6})
NH_2-MIL-125(Ti)	3.17 (3.11)	5.90 (5.88)	3.53 (3.54)	2.37 (2.34)	9.4×10^{-5} (2.7×10^{-4})
(Cu/Ti)1.0 M1	3.12	5.98	4.15	1.83	4.5×10^{-4}
(Cu/Ti)1.0 M2	3.20	6.07	4.27	1.80	3.1×10^{-4}

All the structures displayed in this work were generated using VESTA[22].

References

(1) Zhang, F.; Zhang, B.; Feng, J.; Tan, X.; Liu, L.; Liu, L.; Han, B.; Zheng, L.; Zhang, J.; Tai, J.; Zhang, J. Highly Mesoporous Ru-MIL-125-NH2 Produced by Supercritical Fluid for Efficient Photocatalytic Hydrogen Production. *ACS Appl Energy Mater* 2019, *2* (7), 4964–4970. https://doi.org/10.1021/acsaem.9b00649.

(2) Sun, D.; Liu, W.; Fu, Y.; Fang, Z.; Sun, F.; Fu, X.; Zhang, Y.; Li, Z. Noble Metals Can Have Different Effects on Photocatalysis over Metal-Organic Frameworks (MOFs): A Case Study on M/NH2-MIL-125(Ti) (M=Pt and Au). *Chemistry - A European Journal* 2014, *20* (16), 4780–4788. https://doi.org/10.1002/chem.201304067.

(3) Sun, M.; Yu, F.; Wang, J.; Wang, Y.; Jing, X.; Duan, C. D-NH2-MIL-125 Doped with Cu NPs for Light-Driven Hydrogen Evolution. *Chemical Communications* 2023, *59* (54), 8456–8459. https://doi.org/10.1039/d3cc01770b.

(4) Li, Z.; Xiao, J. D.; Jiang, H. L. Encapsulating a Co(II) Molecular Photocatalyst in Metal-Organic Framework for Visible-Light-Driven H2 Production: Boosting Catalytic Efficiency via Spatial Charge Separation. *ACS Catal* 2016, *6* (8), 5359–5365. https://doi.org/10.1021/acscatal.6b01293.

(5) Nasalevich, M. A.; Becker, R.; Ramos-Fernandez, E. V.; Castellanos, S.; Veber, S. L.; Fedin, M. V.; Kapteijn, F.; Reek, J. N. H.; Van Der Vlugt, J. I.; Gascon, J. Co@NH2-MIL-125(Ti): Cobaloxime-Derived Metal-Organic Framework-Based Composite for Light-Driven H2 Production. *Energy Environ Sci* 2015, *8* (1), 364–375. https://doi.org/10.1039/c4ee02853h.

(6) Martis, M.; Mori, K.; Fujiwara, K.; Ahn, W. S.; Yamashita, H. Amine-Functionalized MIL-125 with Imbedded Palladium Nanoparticles as an Efficient Catalyst for Dehydrogenation of Formic Acid at Ambient Temperature. *Journal of Physical Chemistry C* 2013, *117* (44), 22805–22810. https://doi.org/10.1021/jp4069027.

(7) Kavun, V.; Uslamin, E.; van der Linden, B.; Canossa, S.; Goryachev, A.; Bos, E. E.; Garcia Santaclara, J.; Smolentsev, G.; Repo, E.; van der Veen, M. A. Promoting Photocatalytic Activity of NH2-MIL-125(Ti) for H2 Evolution Reaction through Creation of TiIII- and CoI-Based Proton Reduction Sites. *ACS Appl Mater Interfaces* 2023. https://doi.org/10.1021/acsami.3c15490.

(8) Fu, Y.; Sun, D.; Chen, Y.; Huang, R.; Ding, Z.; Fu, X.; Li, Z. An Amine-Functionalized Titanium Metal-Organic Framework Photocatalyst with Visible-Light-Induced Activity for CO 2 Reduction. *Angewandte Chemie - International Edition* 2012, *51* (14), 3364–3367. https://doi.org/10.1002/anie.201108357.

(9) Fu, Y.; Yang, H.; Du, R.; Tu, G.; Xu, C.; Zhang, F.; Fan, M.; Zhu, W. Enhanced Photocatalytic CO2 Reduction over Co-Doped NH2-MIL-125(Ti) under Visible Light. *RSC Adv* 2017, *7* (68), 42819–42825. https://doi.org/10.1039/c7ra06324e.

(10) Zhao, Y.; Cai, W.; Chen, J.; Miao, Y.; Bu, Y. A Highly Efficient Composite Catalyst Constructed From NH2-MIL-125(Ti) and Reduced Graphene Oxide for CO2 Photoreduction. *Front Chem* 2019, *7*. https://doi.org/10.3389/fchem.2019.00789.

(11) Baluk, M. A.; Pieczyńska, A.; Mazierski, P.; Kroczewska, M.; Nikiforow, K.; Mikolajczyk, A.; Dołżonek, J.; Łuczak, J.; Zaleska-Medynska, A. Effect of Copper and Silver Modification of NH2-MIL-125(Ti) on the Photoreduction of Carbon Dioxide to Formic Acid over This Framework under Visible-Light Irradiation. *Appl Catal B* 2024, *354*. https://doi.org/10.1016/j.apcatb.2024.124107.

(12) Perdew, J. P.; Ruzsinszky, A.; Csonka, G. I.; Vydrov, O. A.; Scuseria, G. E.; Constantin, L. A.; Zhou, X.; Burke, K. Restoring the Density-Gradient Expansion for Exchange in Solids and Surfaces. *Phys Rev Lett* 2008, *100* (13). https://doi.org/10.1103/PhysRevLett.100.136406.

(13) Heyd, J.; Scuseria, G. E.; Ernzerhof, M. Hybrid Functionals Based on a Screened Coulomb Potential. *Journal of Chemical Physics* 2003, *118* (18), 8207–8215. https://doi.org/10.1063/1.1564060.

(14) Schimka, L.; Harl, J.; Kresse, G. Improved Hybrid Functional for Solids: The HSEsol Functional. *Journal of Chemical Physics* 2011, *134* (2). https://doi.org/10.1063/1.3524336.

(15) Kresse, G.; Furthmü, J. *Efficient Iterative Schemes for Ab Initio Total-Energy Calculations Using a Plane-Wave Basis Set*; 1996.

(16) Kresse, G.; Furthmiiller B ', J. *Efficiency of Ab-Initio Total Energy Calculations for Metals and Semiconductors Using a Plane-Wave Basis Set*; 1996; Vol. 6.

(17) Hendon, C. H.; Tiana, D.; Fontecave, M.; Sanchez, C.; D'Arras, L.; Sassoye, C.; Rozes, L.; Mellot-Draznieks, C.; Walsh, A. Engineering the Optical Response of the Titanium-MIL-125 Metal-Organic Framework through Ligand Functionalization. *J Am Chem Soc* 2013, *135* (30), 10942–10945. https://doi.org/10.1021/ja405350u.

(18) Capano, G.; Ambrosio, F.; Kampouri, S.; Stylianou, K. C.; Pasquarello, A.; Smit, B. On the Electronic and Optical Properties of Metal-Organic Frameworks: Case Study of MIL-125 and MIL-125-NH2. *Journal of Physical Chemistry C* 2020, *124* (7), 4065–4072. https://doi.org/10.1021/acs.jpcc.9b09453.

(19) Butler, K. T.; Hendon, C. H.; Walsh, A. Electronic Chemical Potentials of Porous Metal-Organic Frameworks. *J Am Chem Soc* 2014, *136* (7), 2703–2706. https://doi.org/10.1021/ja4110073.

(20) Janak, J. F. *Proof That SE/a n; = e; in Density-Functional Theory*; 1978; Vol. 18.

(21) Sham, L. J.; Schluter, M.; Aboratories, B. I.; Hill, M.; Jersey, N. *PHYSICAL REVIEW LETTERS Density-Functional Theory of the Energy Gay*; 1983; Vol. 51.

(22) Momma, K.; Izumi, F. VESTA 3 for Three-Dimensional Visualization of Crystal, Volumetric and Morphology Data. *J Appl Crystallogr* 2011, *44* (6), 1272–1276. https://doi.org/10.1107/S0021889811038970.